Stator Flux Estimation Based on a Kalman Filter for Stator Flux Vector Control of a Doubly-Fed Induction Motor

Jirawat Kodchaporn and **Warachart Suwan-ngam**†, Non-members

ABSTRACT

Reliable knowledge of the stator flux vector is essential for stator flux vector control of a doubly-fed induction motor (DFIM); therefore, reliable flux estimation is required. Several flux observers have been proposed while the Kalman filter is well known as an optimal state estimator for linear systems. In this paper, a Kalman-filter-based stator flux observer is developed and combined with a double second-order generalized integrator phase-locked loop (DSOGI-PLL) to estimate the flux angular speed and position under non-ideal grid conditions. This work is validated through computer simulation in PLECS software. The CMSIS-DSP library is adopted to perform matrix operations of the Kalman filter. Simulations were performed under different operating conditions, demonstrating that the proposed approach successfully estimates the stator flux vector of the DFIM.

Keywords: Doubly-Fed Induction Motor, Kalman Filter, Stator Flux Estimation, CMSIS-DSP

NOMENCLATURE

DFIM Parameters and Variables:

L_s, L_r	Stator and rotor self-inductances.
L_m	Three-phase magnetizing inductance.
R_s, R_r	Stator and rotor resistances.
$R_r^{'}$	Referred rotor resistance.
τ_s, τ_r	Stator and rotor time constants.
σ	Total leakage factor.
N_s, N_r	Number of stator and rotor turns.
a	Stator-rotor turn ratio.
s	Slip.
P	Number of poles.
$\vec{v}_s, \vec{v}_r$	Stator and rotor voltage vectors.
$\vec{i}_s, \vec{i}_r$	Stator and rotor current vectors.
$\vec{v}_r^{'}, \vec{i}_r^{'}$	Referred rotor voltage and current vectors.
$\vec{v}_s^{\,e}, \vec{v}_r^{'e}$	Stator and referred rotor voltage vectors in the stator flux reference frame.
$\vec{i}_s^{\,e}, \vec{i}_r^{'e}$	Stator and referred rotor current vectors in the stator flux reference frame.
$\vec{i}_s^{\,s}$	Stator current vector in the stationary reference frame fixed to the stator.
$\vec{i}_{ms}^{\,e}$	Stator magnetizing current vector in the stator flux reference frame.
$\vec{\lambda}_s^{\,e}, \vec{\lambda}_r^{'e}$	Stator and referred rotor flux vectors in the stator flux reference frame.
i_{sd}^e, i_{sq}^e	D-axis and Q-axis stator currents in the stator flux reference frame.
$i_{rd}^{'e}, i_{rq}^{'e}$	D-axis and Q-axis rotor currents in the stator flux reference frame.
$v_{rd}^{e"}, v_{rq}^{e"}$	D-axis and Q-axis PWM command voltages in the stator flux reference frame.
ω_e	Stator flux speed, Synchronous speed.
ω_r, ω_{rm}	Rotor electrical and mechanical angular speeds.
ω_{sl}	Slip speed.
τ_m	Mechanical Time constant.
T_e	Electromagnetic torque.
T_L	Load torque.

Kalman Filter Variables:

A, B, C	System matrix, input matrix and output matrix.
A_{k-1}	State-transition matrix.
B_{k-1}	Input matrix.
K_k	Kalman gain.
$\hat{x}_0^+$	Mean of initial state.
$\hat{P}_0^+$	Mean of initial covariance.
P_k^-, P_k^+	Priori and posteriori covariance matrices.
$\hat{x}_k^-, \hat{x}_k^+$	Priori and posteriori state estimates.
y_k	Measurement vector.
Q	Process noise covariance.
R	Measurement noise covariance.
I	Identity matrix.
v	Measurement noise.
w	System noise.
δ	Kronecker delta.

Manuscript received on March 31, 2025; revised on May 16, 2025; accepted on May 22, 2025. This paper was recommended by Associate Editor Chainarin Ekkaravarodome.

The authors are with Department of Electrical Engineering, School of Engineering, King Mongkut's Institute of Technology Ladkrabang, Thailand.

†Corresponding author: warachart.su@kmitl.ac.th

Digital Object Identifier: 10.37936/ecti-eec.2525232.258565

1. INTRODUCTION

Vector control is a high-performance control for electric machines. Reference frame estimation is mandatory to achieve the task. In the case of an induction machine, the rotor-flux vector is generally selected as a reference vector to create the reference frame [1-6]. However, in the case of a doubly-fed induction machine, the stator-flux linkage is generally used as the reference vector for creating the reference frame [1-5, 11, 12]. Alternatively, in the application as a doubly-fed induction generator (DFIG), the grid-voltage or grid-flux reference frame is generally applied for active-and reactive-power control [12]. However, the stator-flux reference frame is generally applied to the application as a doubly-fed induction motor (DFIM) [13-17].

Several methods, called flux observers, have been proposed to estimate the rotor-flux vector for vector control of induction machines. The flux observers applied to the induction machine can also be applied to the DFIM. They can be classified as open-loop and closed-loop observers. The principal difference between open-loop and closed-loop observers is that the estimated states of closed-loop observers are corrected by corrective feedback included. For this process, the measured outputs are compared to the outputs calculated from the estimated states. The error results are fed back to minimize the estimation errors.

The voltage model, current model, the full–order forward observer and the cancellation method are classified as open-loop observers [1-5]. The voltage model has a simple structure and is affected by the stator parameters only. However, due to the integration of the stator back-EMF, it does suffer from a small dc offset [8, 10]. Although this problem can simply be solved by using a low cut-off frequency (1-5 Hz) low-pass filter, some problems about phase-shift and gain still exist [10]. The current model is another simple method, but it is highly dependent on the parameters. The full-order forward observer can estimate more state variables apart from the stator-flux linkage, depending on the DFIM dynamic model. This method provides full DFIM dynamics, but, due to open-loop structure, the estimation errors can accumulate gradually. The cancellation method provides instantaneous response, but it can amplify noise due to its derivative structure.

Luenberger observer, MRAS observer, sliding-mode observer and the Kalman-filter family are classified as closed-loop observers. They have been applied to estimate not only the rotor flux but also the rotor speed and position for sensorless control, providing superior estimation results compare with those of open-loop observers [7-10]. The Luenberger observer is computationally inexpensive due to simple matrix manipulation [18]. It also provides smooth estimated signals without chattering, as presented in the case of the sliding-mode observer. However, its parameter sensitivity can degrade its accuracy. The MRAS observer requires only two open-loop models, the reference and adaptive models, and a PI controller to complete flux estimation. It is best suited for small-size microcontrollers. However, if the reference model is integrator-based, as in the case of the classical voltage model, a modification is required [19-21]. Parameter mismatch, especially magnetizing inductance and stator inductance, affects the performance of this observer [22-25]. PI-controller tuning is one of the drawbacks of the MRAS observer. Poorly tuning controller gains can slow convergence, requiring adaptive tuning or an alternative method based on the recursive-least-square technique to solve this problem [25]. The sliding-mode observer provides fast dynamic response. It is also robust to parameter drift. However, as reported in some papers, there is high frequency oscillation, called “chattering”, results in torque pulsation, so the smoothing filter or extensive chattering suppression technique are required [26-28]. There must be a trade-off between smoothness and bandwidth. All these observers suffer from measurement noise, so there must be some modification to mitigate the noise. Conversely, the Kalman filter incorporates noise in the model, the measurement noise is suppressed by the Kalman gain in its algorithm.

The Kalman filter is an optimal state estimator [29] for linear systems. The nonlinear version, called the extended Kalman filter (EKF), is used for parameter estimation and speed-sensorless control [2-5, 30-32]. However, in this paper, only the standard Kalman filter is adequate because parameters drift is not considered, and the DFIM model consisting of four state variables is applied to estimate the stator-flux vector. A major drawback of the Kalman filter is its high computational burden, largely caused by the repeated matrix manipulation, especially matrix inversion, required at each step [2-5]. It was previously not suitable for the low-cost low performance drive system. However, with advancements in semiconductor technology, this drawback has been mitigated.

This paper proposes the stator-flux-vector estimation scheme based on a Kalman filter integrated with a dual second-order generalized integrator phase-locked loop (DSOGI-PLL). The Kalman filter estimates the d- and q-axis stator-flux components in the stator-flux reference frame. Due to non-ideal grid voltage, especially unbalanced voltage, the estimated stator flux is distorted, which consequently distorts the estimated stator-flux speed and position. Therefore, the DSOGI-PLL is applied to estimate the flux speed and position for the positive-sequence stator-flux component. Consequently, the results are smoothed, as shown in the simulation results.

The key contribution of this paper is to validate the stator-flux estimation scheme using a Kalman filter integrated with a DSOGI-PLL via PLECS simulation software. The stator-flux estimation and vector control modules are coded in C-Script block to emulate the code which will be applied to the ARM-based microcontroller system.

This paper begins with a discussion of a mathematical

model of a DFIM and the concept of the Kalman filter in Section 2. Section 3 focuses on the estimated stator-flux vector based on a Kalman filter combined with a DSOGI-PLL. The stator-flux estimation system is validated through simulation under different operating conditions using PLECS software, as discussed in Section 4. The simulation results are also presented and discussed in this section. Finally, the conclusion is presented in Section 5.

2. MATHEMATICAL MODEL OF STATOR FLUX VECTOR ESTIMATION FOR A DOUBLY-FED INDUCTION MOTOR

The 1^{st} order differential equations of the rotor current and stator flux vectors for a DFIM under stator flux vector control are shown in equations (1) and (2) respectively,

$$\sigma\tau_r \frac{d\vec{i}_r^{\,\prime e}}{dt} + \vec{i}_r^{\,\prime e} = \frac{\vec{v}_r^{\,\prime e}}{R_r^{\,\prime}} - j\omega_{sl}\sigma\tau_r \vec{i}_r^{\,\prime e} - \frac{(1-\sigma)\tau_r}{L_m}\left(\frac{d\vec{\lambda}_s^e}{dt} + j\omega_{sl}\vec{\lambda}_s^e\right), \tag{1}$$

$$\tau_s \frac{d\vec{\lambda}_s^e}{dt} + \vec{\lambda}_s^e = \tau_s \vec{v}_s^e + L_m \vec{i}_r^{\,\prime e} - j\omega_e \tau_s \vec{\lambda}_s^e, \tag{2}$$

while $\sigma = 1 - \frac{L_m^2}{L_s L_r'}$, and $\omega_{sl} = \omega_e - \omega_r$.

The electromagnetic torque and mechanical dynamic equations are presented in equations (3) and (4) respectively,

$$T_e = \frac{P}{2}\frac{3}{2}\frac{L_m}{L_s}\left(\lambda_{sq}^e i_{rd}^{\prime e} - \lambda_{sd}^e i_{rq}^{\prime e}\right), \tag{3}$$

$$\tau_m \frac{d\omega_{rm}}{dt} + \omega_{rm} = T_e - T_L. \tag{4}$$

The stator flux linkage can be expressed in the form of the product of the three-phase magnetizing inductance and the stator magnetizing current as shown in equation (5),

$$\vec{\lambda}_s^e = L_m \vec{i}_{ms}^e. \tag{5}$$

Since stator flux vector control is performed in the stator flux reference frame, only the d-axis component of the stator flux linkage, which is equal to the amplitude of the stator flux vector, exists, so the equation of the electromagnetic torque can be derived as shown in equation (6),

$$T_e = -\frac{P}{2}\frac{3}{2}\frac{L_m^2}{L_s}\left|\vec{i}_{ms}^e\right| i_{rq}^{\prime e}. \tag{6}$$

The control diagram of the DFIM using the Kalman filter for stator flux estimation is shown in Fig.1.

As can be seen in Fig. 1, the PI controllers are used to control the rotor circuit of the DFIM. The feed-forward compensation method is applied to cancel the cross-coupling voltage appearing in equation (1). The compensating voltages in each axis are depicted in equations (7) and (8) respectively,

$$v_{comp\_d} = -\omega_{sl}\sigma\tau_r i_{rq}^{\prime e} + (1-\sigma)\tau_r \frac{d\left|\vec{i}_{ms}^e\right|}{dt}, \tag{7}$$

$$v_{comp\_q} = \omega_{sl}\sigma\tau_r i_{rd}^{\prime e} + \omega_{sl}(1-\sigma)\tau_r \left|\vec{i}_{ms}^e\right|. \tag{8}$$

Therefore, the command voltages which are then transformed back to three-phase commands to generate PWM signals are as follows,

$$v_{rd}^{e\prime\prime} = v_{rd}^{e\prime} + v_{comp\_d}, \tag{9}$$

$$v_{rq}^{e\prime\prime} = v_{rq}^{e\prime} + v_{comp\_q}. \tag{10}$$

These command voltages are used as the input variables for the stator flux vector estimation.

2.1 Mathematical Model of the DFIM

Stator flux vector estimation using the Kalman filter requires a mathematical model in the state-space form. However, the 5^{th} order model of the DFIM is nonlinear due to the multiplication of the state variables in the equation, so the general form can be described as shown in equation (11),

$$\dot{x} = f(x, u, w, t). \tag{11}$$

The 1^{st} order differential equations of each state in the stator flux reference frame are shown in equations (12)-(16). The input variables of the electrical equations are the stator voltage and rotor voltage in their own reference frames. The equation of the electrical rotor speed described in equation (16) is derived from equations (3) and (4). It should be noted that there are multiplications of all first four state variables, appearing in the first two terms on the right-hand side of equation (16), resulting in a nonlinear state equation.

$$\begin{aligned}\frac{di_{rd}^{\prime e}}{dt} = &-\left(\frac{1}{\sigma\tau_r} + \frac{1-\sigma}{\sigma\tau_s}\right) i_{rd}^{\prime e} + (\omega_e - \omega_r) i_{rq}^{\prime e} \\ &+ \frac{(1-\sigma)}{\sigma\tau_s L_m}\lambda_{sd}^e - \omega_r \frac{(1-\sigma)}{\sigma L_m}\lambda_{sq}^e \\ &- \frac{(1-\sigma)}{\sigma L_m}\cos\theta_e v_{sd}^s - \frac{(1-\sigma)}{\sigma L_m}\sin\theta_e v_{sq}^s \\ &+ \frac{1}{\sigma L_r^{\prime}}\cos(\theta_e - \theta_r) v_{rd}^{\prime r} \\ &+ \frac{1}{\sigma L_r^{\prime}}\sin(\theta_e - \theta_r) v_{rq}^{\prime r},\end{aligned} \tag{12}$$

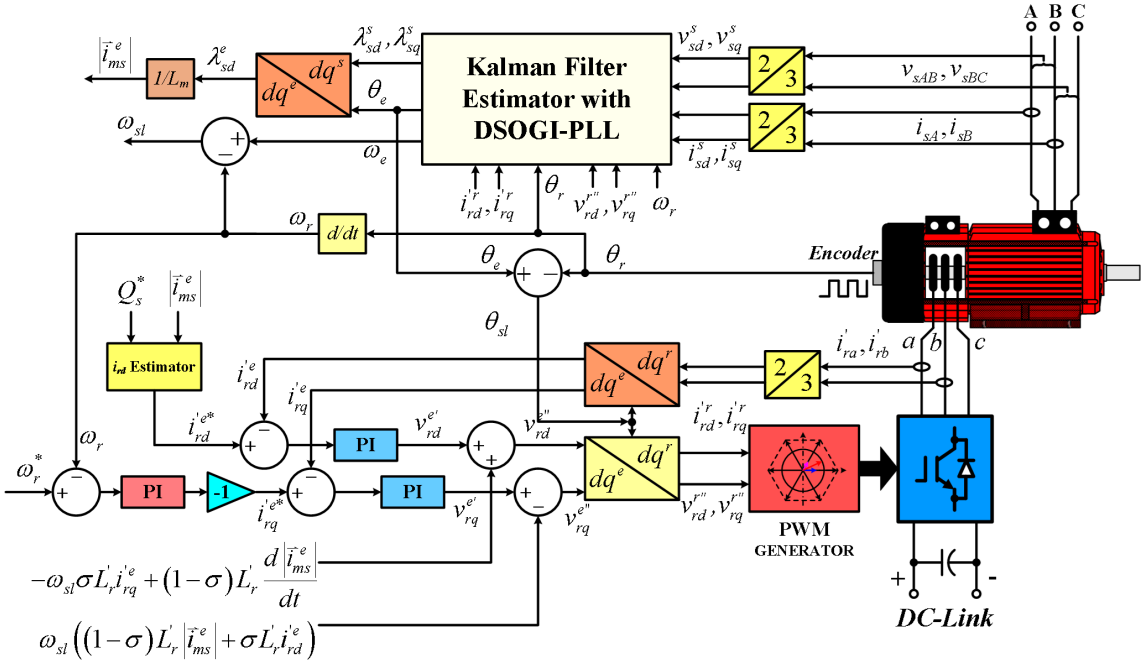

***Fig. 1**: Control Diagram of the DFIM using the Kalman Filter with DSOGI-PLL for Stator Flux Vector Estimation.*

$$\begin{aligned}\frac{di'^{e}_{rq}}{dt} &= -(\omega_e-\omega_r)i'^{e}_{rd} - \left(\frac{1}{\sigma\tau_r}+\frac{1-\sigma}{\sigma\tau_s}\right)i'^{e}_{rq}\\ &+\omega_r\frac{(1-\sigma)}{\sigma L_m}\lambda^{e}_{sd}+\frac{(1-\sigma)}{\sigma\tau_s L_m}\lambda^{e}_{sq}\\ &+\frac{(1-\sigma)}{\sigma L_m}\sin\theta_e v^{s}_{sd}-\frac{(1-\sigma)}{\sigma L_m}\cos\theta_e v^{s}_{sq}\\ &-\frac{1}{\sigma L'_r}\sin(\theta_e-\theta_r)v'^{r}_{rd}\\ &+\frac{1}{\sigma L'_r}\cos(\theta_e-\theta_r)v'^{r}_{rq},\end{aligned} \tag{13}$$

$$\begin{aligned}\frac{d\lambda^{e}_{sd}}{dt} &= \frac{L_m}{\tau_s}i'^{e}_{rd}-\frac{1}{\tau_s}\lambda^{e}_{sd}+\omega_e\lambda^{e}_{sq}\\ &+\cos\theta_e v^{s}_{sd}+\sin\theta_e v^{s}_{sq},\end{aligned} \tag{14}$$

$$\begin{aligned}\frac{d\lambda^{e}_{sq}}{dt} &= \frac{L_m}{\tau_s}i'^{e}_{rq}-\omega_e\lambda^{e}_{sd}-\frac{1}{\tau_s}\lambda^{e}_{sq}\\ &-\sin\theta_e v^{s}_{sd}+\cos\theta_e v^{s}_{sq},\end{aligned} \tag{15}$$

$$\begin{aligned}\frac{d\omega_r}{dt} &= \frac{3}{2J}\left(\frac{P}{2}\right)^2\frac{L_m}{L_s}\lambda^{e}_{sq}i'^{e}_{rd}\\ &-\frac{3}{2J}\left(\frac{P}{2}\right)^2\frac{L_m}{L_s}\lambda^{e}_{sd}i'^{e}_{rq}\\ &-\frac{B}{J}\omega_r-\frac{P}{2J}T_L.\end{aligned} \tag{16}$$

Since the rotor speed and position signals are measured using an incremental encoder, and parameter variation due to either magnetic saturation or temperature is neglected, the DFIM model is reduced to the 4^{th} order model containing only electrical states such as i'^{e}_{rd}, i'^{e}_{rq}, λ^{e}_{sd}, and λ^{e}_{sq} respectively. The DFIM model can be represented by a linear-time-varying model as shown in equation (17),

$$\dot{x} = A(t)x(t)+B(t)u(t). \tag{17}$$

Following this assumption, the linear observer is sufficient to estimate the stator flux linkage vector components, λ^{e}_{sd}, and λ^{e}_{sq}. Therefore, the standard Kalman filter is suitable for this task, and the details are discussed in the next sub-section.

2.2 Discrete-Time Kalman Filter

The Kalman filter is a recursive state estimator which can be used for estimating the internal states of the system. It can provide the optimal state estimate although the system and measurements are noisy. This algorithm consists of two steps: prediction and update. The prediction step is to predict the states using the model. This step is called "Time Update". The predicted states are then corrected by comparing them to the measurement data using the Kalman gain. This step is called "Measurement Update". The dynamic system can be described as follows,

$$\begin{aligned}x_k &= A_{k-1}x_{k-1}+B_{k-1}u_{k-1}+w_{k-1}\\ y_k &= C_k x_k+v_k\\ E\left[w_k w_j^T\right] &= Q_k\delta_{k-j}\\ E\left[v_k v_j^T\right] &= R_k\delta_{k-j}\\ E\left[v_k w_j^T\right] &= 0,\end{aligned} \tag{18}$$

while w_{k-1} is the process noise matrix and v_k is the measurement noise matrix. The process noise and measurement noise are assumed to be uncorrelated as described in $E\left[v_k w_j^T\right] = 0$.

An alternative form of the Kalman filter, called the Extended Kalman Filter (EKF), is generally applied to estimate the states as well as parameters in the cases of nonlinear phenomena, for example, parameter drift due to changes in the temperature and magnetic saturation is considered. Additionally, speed-sensorless motor control is an application that requires a nonlinear Kalman filter. The EKF requires the online calculation of the Jacobians of the nonlinear system matrix for the calculation of the covariance matrix and Kalman gain. However, in the case of the linear-time-varying system as discussed in this paper, the Jacobians are identical to the system and output matrices. Therefore, the Kalman filter is sufficient for this application. The algorithm can be explained as follows.

1. Initialization:
The algorithm starts from initialization for the state and noise covariance as depicted in equation (19),

$$\begin{aligned} \hat{x}_0^+ &= E(x_0) \\ P_0^+ &= E\left[(x_0 - \hat{x}_0^+)(x_0 - \hat{x}_0^+)^T\right]. \end{aligned} \tag{19}$$

The $\hat{x}_0^+$ and P_0^+ are the means of the initialized state and noise covariance.

2. Time update:
Once the state and covariance are initialized, the present state and covariance are first predicted in this step. The prediction is based on the model of the system, the state-transition matrix and input matrix. The results of this step are $\hat{x}_k^-$ and P_k^- which are called a priori state estimate and a priori covariance. The process of this step is depicted in equation (20),

$$\begin{aligned} \hat{x}_k^- &= A_{k-1}\hat{x}_{k-1}^+ + B_{k-1}u_{k-1} \\ P_k^- &= A_{k-1}P_{k-1}^+ A_{k-1}^T + Q_{k-1}. \end{aligned} \tag{20}$$

3. Measurement update:
In this step, the predicted states are corrected by the measurement output. The priori covariance is used to calculate the Kalman gain for the correction of the state estimates. Calculation of the Kalman gain, covariance and corrected state estimates is shown in equation (21),

$$\begin{aligned} K_k &= P_k^- C_k^T \left(C_k P_k^- C_k^T + R_k\right)^{-1} \\ \hat{x}_k^+ &= \hat{x}_k^- + K_k(y_k - C_k\hat{x}_k^-) \\ P_k^+ &= (I - K_k C_k)P_k^-(I - K_k C_k)^T + K_k R_k K_k^T. \end{aligned} \tag{21}$$

The state estimates and covariance $\hat{x}_k^+$ and P_k^+ are called a posteriori state and a posteriori covariance respectively. These values are then used for the time-update step in the next sampling. All the processes can be summarized in the flowchart shown in Fig. 2.

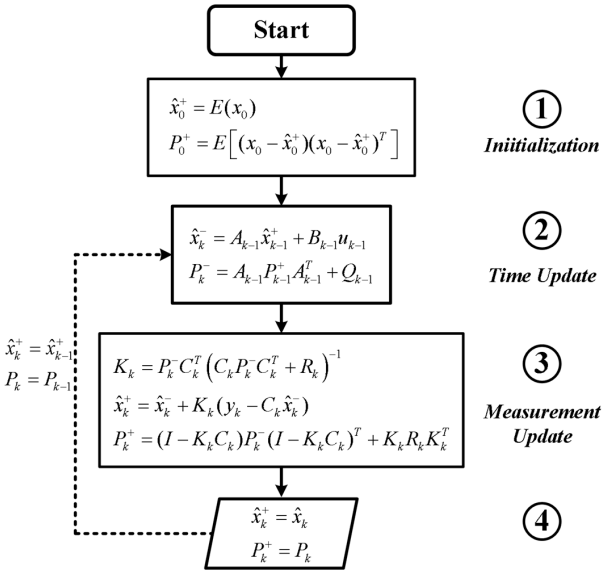

***Fig. 2**: A Flowchart of the Kalman-Filter Estimator.*

3. STATOR FLUX VECTOR ESTIMATION USING KALMAN FILTER

The stator flux vector estimation consists of the process of estimating λ_{sd}^e, and λ_{sq}^e and estimating the flux position and angular speed. The estimation of the dq components is achieved by a discrete-time Kalman filter while the flux position and angular speed estimation is achieved by the DSOGI-PLL.

3.1 Kalman Filter Based Stator Flux Estimation

Since simulation and implementation are performed in the discrete-time domain, it is necessary to discretize the system before processing the estimation. The simple method usually applied to the system is the 1^{st} order Taylor's approximation. The approximate discrete value is shown in equation (22),

$$\dot{x} \approx \frac{x_k - x_{k-1}}{T_s}. \tag{22}$$

An increase in both sampling frequency and order of approximation helps improve approximation accuracy. However, there must be a trade-off between the computational burden and approximation accuracy. In this research, the sampling frequency is 10 kHz which is high enough for the 1^{st} approximation as reported in [6]. The discrete-state space equations for state estimation using the discrete-time Kalman filter are depicted in equations (23) and (24),

$$x_k = A_{k-1}x_{k-1} + B_{k-1}u_{k-1} + w_{k-1} \tag{23}$$

$$y_k = C_k x_k + v_k \tag{24}$$

The details of the state and input vectors as well as the state and input transition matrices are depicted in equations (25) – (28),

$$x_{k-1} = \begin{bmatrix} i'^e_{rd,k-1} & i'^e_{rq,k-1} & \lambda^e_{sd,k-1} & \lambda^e_{sq,k-1} \end{bmatrix}^T \tag{25}$$

$$u_{k-1} = \begin{bmatrix} v^s_{sd,k-1} & v^s_{sq,k-1} & v'^r_{rd,k-1} & v'^r_{rq,k-1} \end{bmatrix}^T \quad (26)$$

$$A_{k-1} = \begin{bmatrix} 1-a_1 & a_2 & a_3 & -a_4 \\ -a_2 & 1-a_1 & a_4 & a_3 \\ a_5 & 0 & 1-a_6 & a_7 \\ 0 & a_5 & -a_7 & 1-a_6 \end{bmatrix} \quad (27)$$

$$B_{k-1} = \begin{bmatrix} -b_1 & -b_2 & b_3 & b_4 \\ b_2 & -b_1 & -b_4 & b_3 \\ b_5 & b_6 & 0 & 0 \\ -b_6 & b_5 & 0 & 0 \end{bmatrix} \quad (28)$$

while

$$a_1 = T_s\left(\frac{1}{\sigma\tau_r} + \frac{1-\sigma}{\sigma\tau_s}\right), a_2 = T_s(\omega_e - \omega_r),$$

$$a_3 = T_s\frac{(1-\sigma)}{\sigma\tau_s L_m}, a_4 = T_s\omega_r\frac{(1-\sigma)}{\sigma L_m},$$

$$a_5 = T_s\frac{L_m}{\tau_s}, a_6 = T_s\frac{1}{\tau_s},$$

$$a_7 = T_s\omega_e,$$

$$b_1 = T_s\frac{(1-\sigma)}{\sigma L_m}\cos\theta_e, b_2 = T_s\frac{(1-\sigma)}{\sigma L_m}\sin\theta_e,$$

$$b_3 = T_s\frac{1}{\sigma L'_r}\cos(\theta_e - \theta_r),$$

$$b_4 = T_s\frac{1}{\sigma L'_r}\sin(\theta_e - \theta_r),$$

$$b_5 = T_s\cos\theta_e, b_6 = T_s\sin\theta_e.$$

Likewise, the output vector and output matrix are shown in equations (29) and (30) respectively,

$$y_k = \begin{bmatrix} i'^r_{rd,k} & i'^r_{rq,k} & i^s_{sd,k} & i^s_{sq,k} \end{bmatrix}^T \quad (29)$$

$$C_k = \begin{bmatrix} c_1 & -c_2 & 0 & 0 \\ c_2 & c_1 & 0 & 0 \\ -c_3 & c_4 & c_5 & -c_6 \\ -c_4 & -c_3 & c_6 & c_5 \end{bmatrix} \quad (30)$$

while

$$c_1 = \cos(\theta_e - \theta_r), c_2 = \sin(\theta_e - \theta_r),$$

$$c_3 = \frac{L_m}{L_s}\cos\theta_e, c_4 = \frac{L_m}{L_s}\sin\theta_e,$$

$$c_5 = \frac{1}{L_s}\cos\theta_e, c_6 = \frac{1}{L_s}\sin\theta_e.$$

In this research, the rotor input voltages are from the PI controller command as depicted in equations (9) and (10). Since only the i'^e_{rd}, i'^e_{rq}, λ^e_{sd}, and λ^e_{sq} are estimated, only the 4×4 matrix consisting of electrical states is adequate. The Jacobians of both state and output transition matrices are identical to the state and output transition matrices themselves. Moreover, the effect of parameter variation is not considered. Therefore, it is not necessary to use the extended Kalman filter for this task.

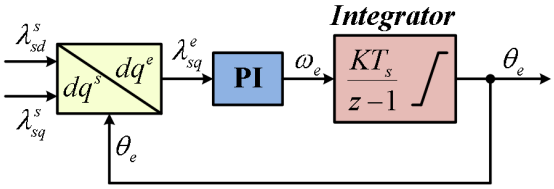

***Fig. 3**: Block Diagram of the DQ-PLL.*

The Q and R matrices are tuned to achieve the satisfactory results in both transient and steady states. The values of Q and R are as follows,

$$Q = diag\left(\begin{bmatrix} 1.37e^{-1} & 1.37e^{-1} & 1.04e^{-2} & 1.04e^{-2} \end{bmatrix}\right),$$

$$R = diag\left(\begin{bmatrix} 1.37e^{-2} & 1.37e^{-2} & 1.37e^{-2} & 1.37e^{-2} \end{bmatrix}\right).$$

The diagonal elements of Q are set to 1 % of the base value of the state while the diagonal elements of R are set to 0.1 % of the base value of the input variables. The initial value of P is $P = diag\left(\begin{bmatrix} 1 & 1 & 1 & 1 \end{bmatrix}\right)$.

3.2 A DSOGI-PLL for Position and Angular Speed Estimation

Once the Kalman filter process is finished, the stator flux λ^e_{sd} and λ^e_{sq} are transformed into the stationary reference frame fixed to the stator providing λ^s_{sd} and λ^s_{sq} respectively to estimate the angular speed and position of the stator flux vector. In the case of an ideal grid voltage, the dq phase-locked loop (dq-PLL), which is generally used for grid synchronization of the grid-connected three-phase converters, is applied to the stator flux linkage vector as shown in Fig. 3.

The estimated angular speed and position of the stator flux vector, using the dq-PLL, become distorted if the grid disturbances, for example harmonic distortion and unbalanced grid voltage, do occur. The effect of harmonic voltage can be mitigated by reducing the bandwidth of the dq-PLL [33]. However, the effect of unbalanced voltage cannot be solved by this method. The unbalanced voltage can directly affect the estimated stator flux because the stator of the DFIM is directly connected to the grid. Based on the instantaneous symmetrical component (ISC) method, the DSOGI with the positive-sequence calculation (PSC) can isolate the positive sequence component from the negative sequence component, as depicted in Fig. 4.

The DSOGI with PSC behaves as a low-pass filter for the positive-sequence component, and behaves as a notch filter for the negative-sequence component [33, 34]. Therefore, only the positive-sequence flux components, λ^{s+}_{sd} and λ^{s+}_{sq} are then fed to the dq-PLL providing the smooth estimated angular speed and position. The stator flux vector estimation based on the Kalman filter with DSOGI-PLL is illustrated in Fig. 5. The estimated angular speed, ω_e is fed back to the DSOGI-QG blocks to adapt the resonant frequency as discussed in [33].

***Table 1**: Parameters of a WRIM.*

Parameter	Value	Unit	Parameter	Value	Unit
Stator Rated Voltage	400	V	Stator Resistance	1.0972	Ω
Rotor Rated Voltage	200	V	Referred Rotor Resistance	2.0250	Ω
Stator Rated Current	9.7	A	Stator Self Inductance	0.203642	H
Rotor Rated Current	11.4	A	Referred Rotor Self Inductance	0.203642	H
Base Frequency	50	Hz	Magnetizing Inductance	0.195853	H
Base Speed	1500	rpm	Moment of Inertia	0.018	kg·m^2
Number of Poles	4	Poles	Viscous Friction Coefficient	0.008242	N·m·s rad^{-1}
Stator-Rotor Turn Ratio	2		DC Bus Voltage	300	V

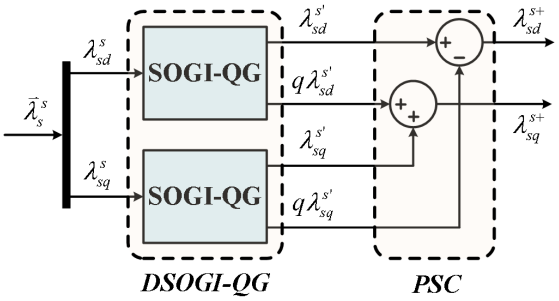

***Fig. 4**: Block Diagram of the DSOGI and PSC.*

4. SIMULATION AND SIMULATION RESULTS

The computer simulations were performed to validate the application of the Kalman filter for stator flux vector estimation. The details of the simulation system are described in sub-section 4.1.

4.1 Simulation System

The non-saturable model of a 5 kW wound-rotor induction machine having the variables and parameters as shown in Table 1 is used in the simulation. The PLECS software is applied to simulate the stator flux estimation system having the diagram depicted in Fig. 6. In the simulation, the operation criteria of the DFIM are discussed in [35, 36].

The machine-side converter (MSC) is controlled with a sampling rate of 10 kHz, while the switching frequency is set to 5 kHz. As a result, the PWM signals are updated twice for each switching period. The simulation was performed using C-Script as applied in the actual system.

The series PI controller, having the structure shown in Fig. 7, is applied to both current and speed control loops. The transfer function $G_c(s)$ of this PI controller is shown in equation (31),

$$G_c(s) = K_a + \frac{K_a K_b}{s}, \tag{31}$$

while K_a is the series gain and K_b is the inflection frequency [37].

As discussed in [37], the controller gain K_a is used to adjust the bandwidth of the closed-loop system. On the other hand, adjusting K_b does reflect the inflection frequency without increasing the gain at high frequency. The relationship between K_a, K_b and K_P, K_I of the parallel structure is shown in equations (32) and (33) respectively [36],

***Table 2**: Controller Gains and Bandwidth of the Current and Speed Control Loops. [36]*

Controller Parameters	Current Loop	Speed Loop
K_a	2.5	2
K_b	200 s^{-1}	10 s^{-1}
Bandwidth	629.58 Hz	7.15 Hz

$$K_P = K_a, \tag{32}$$

$$K_I = K_a K_b. \tag{33}$$

The controller gains of the current control loops are identical for both d and q axes. The controller gains and bandwidths for the speed and current control loops are described in Table 2.

The frequency responses for the current control loop and the speed control loop are shown in Figs. 8 and 9 respectively.

The CMSIS-DSP library used for ARM-based microcontrollers is adopted to perform the matrix manipulation required for the Kalman filter algorithm. It can help optimize the code and can be directly transferred to the hardware implementation step with little modification. The simulations were performed under a 1 pu load condition. The operating speed is set to 1.2 pu. The rotor is responsible for magnetizing the DFIM, meaning that the stator reactive power is controlled to be zero. The simulation results were plotted using MATLAB software.

4.2 Simulation Results

The simulations results are classified into four groups such as 1. Step change in speed command, 2. Step change in load torque, 3. Operation in generator mode and 4. Operation under unbalanced stator voltage. The main results focus on the comparison of stator flux waveforms in the stationary reference frame fixed to the stator, between the reference waveforms from the model probe and the estimated waveforms from the Kalman filter. The

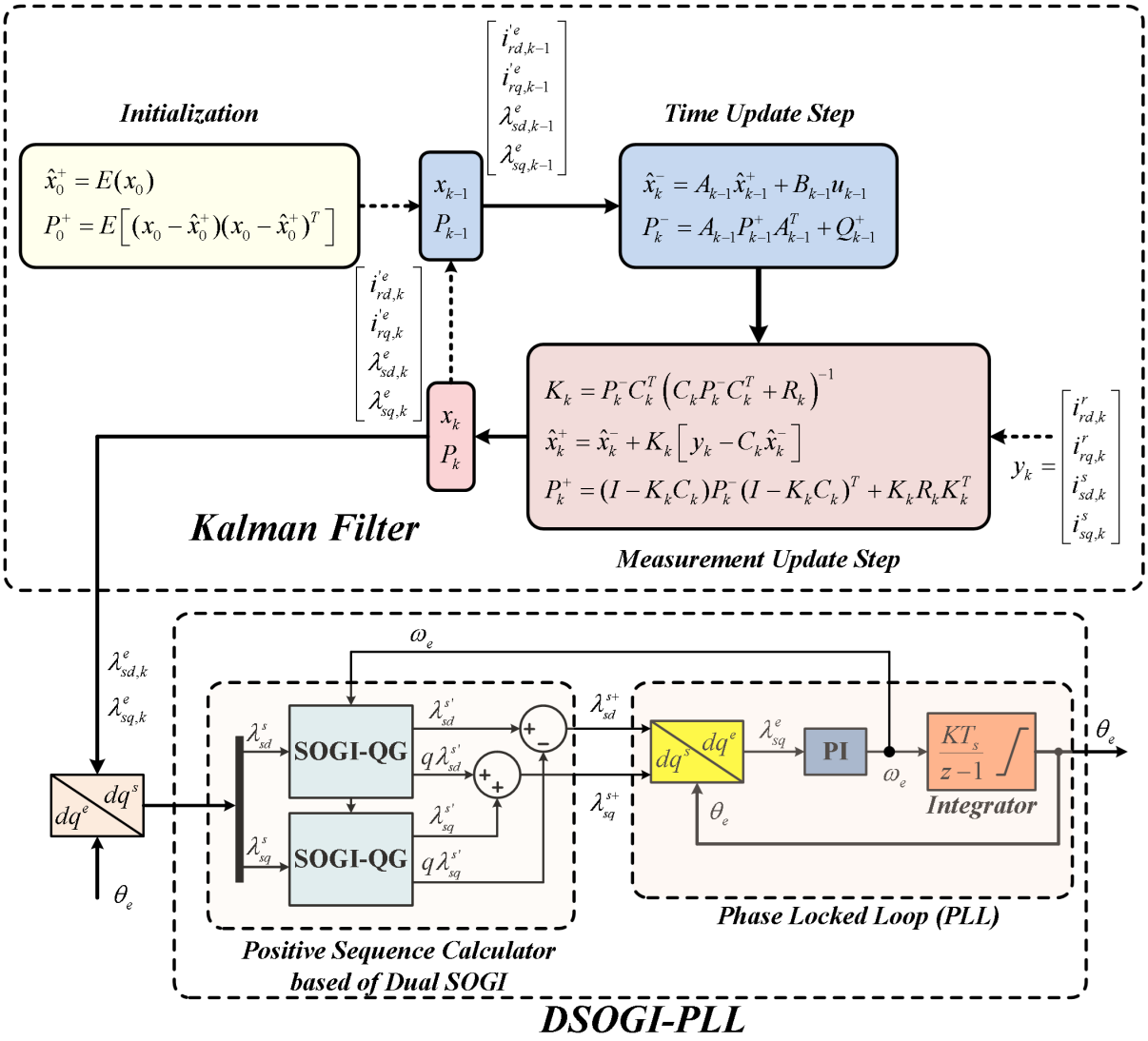

***Fig. 5**: Stator Flux Vector Estimation Block Diagram using Kalman Filter with DSOGI-PLL.*

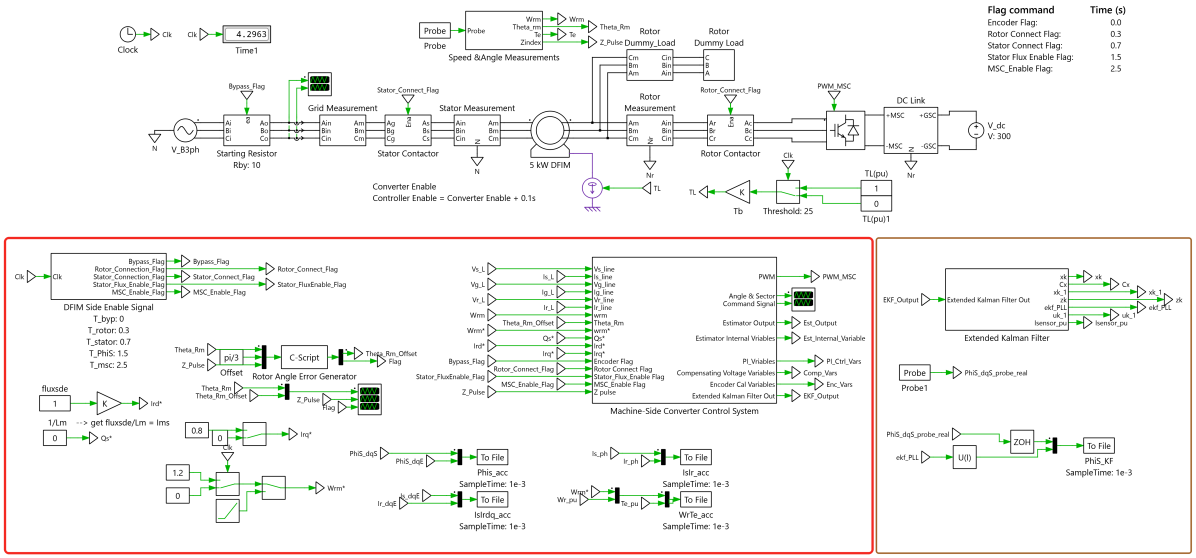

***Fig. 6**: Simulation Diagram of the Proposed Stator-Flux Estimation Scheme for the DFIM.*

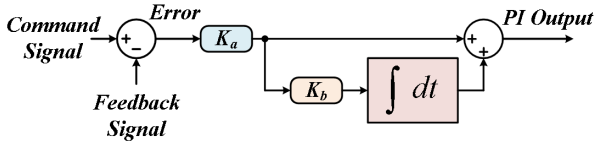

***Fig. 7**: Series PI Controller Structures.*

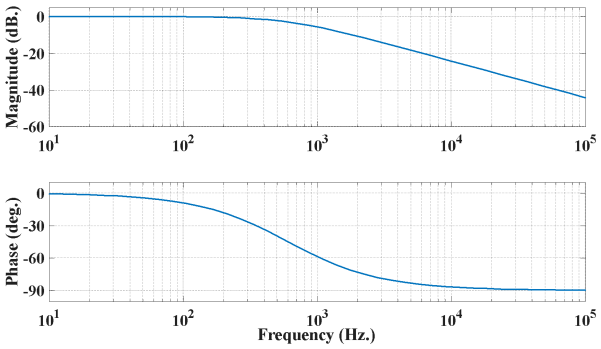

***Fig. 8**: The Bode Plot for the Closed-Loop Transfer Function of the Current Control Loop. [36]*

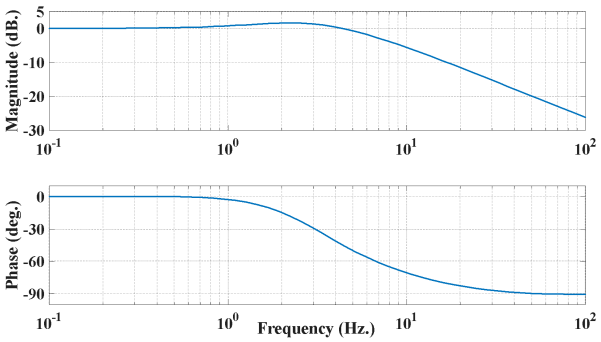

***Fig. 9**: The Bode Plot for the Closed-Loop Transfer Function of the Speed Control Loop. [36]*

root-mean-square (RMS) error is applied to calculate the deviation of the estimated flux from the reference flux. The RMS error equation is shown in equation (34),

$$\lambda_s^s RMSE = \sqrt{\frac{1}{N}\sum_{k=1}^{N}\left(\lambda_s^s[k] - \hat{\lambda}_s^s[k]\right)^2} \qquad (34)$$

while $N = T_1/T_{samp}$, $T_1 = 0.02\ s$ and $T_{samp} = 0.0001\ s$.

4.2.1 Step Change in Speed Command

The simulation results begin with the stator flux waveform during the enabling of the stator flux estimation as shown in Fig.10. During this step, only the stator is connected to the grid while the rotor is open-circuited. The rotor speed remains zero as shown in the bottom waveforms. As shown in this figure, the reference and the estimated waveforms coincide.

The results shown in Figs. 11 and 12 are the waveforms during the step change in the speed command

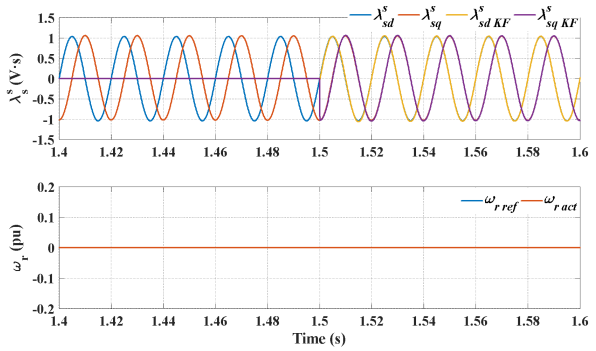

***Fig. 10**: Simulation Results Showing the Waveforms of the (Top) Stator Flux and (Bottom) Rotor Speed during Enabling of Stator Flux Estimation.*

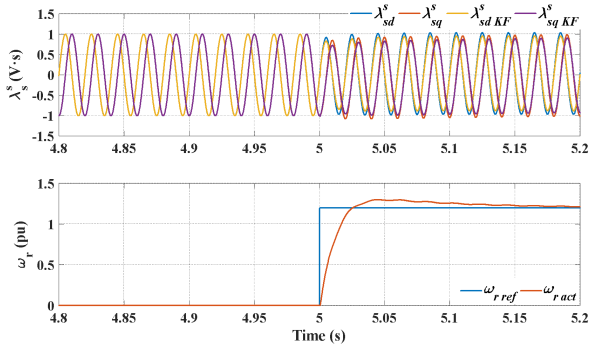

***Fig. 11**: Simulation Results Showing the Waveforms of the (Top) Stator Flux and (Bottom) Rotor Speed during a Step Change in Speed Command.*

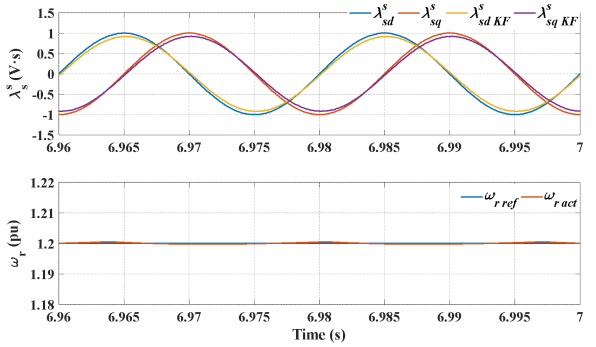

***Fig. 12**: Simulation Results Showing the Waveforms of the (Top) Stator Flux and (Bottom) Rotor Speed under Steady-State Motor Operation.*

and the steady-state condition respectively. During the step change at 5 s, the estimated stator flux waveforms have the same response as the reference flux waveforms. There are slight differences in the amplitude of the stator flux waveforms as shown in both figures.

A magnified view of the stator flux waveforms is shown in Fig. 13, There is also a small phase delay occurring in the estimated waveform. Both differences in amplitude and phase angle can be solved by increasing

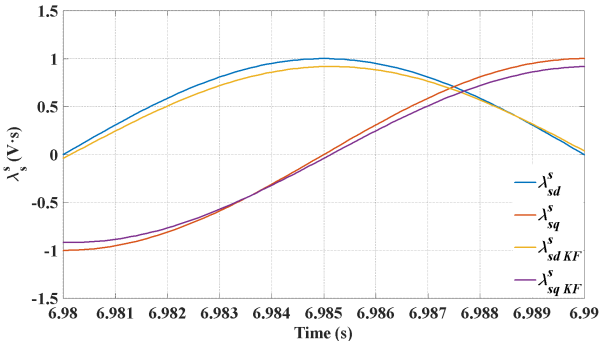

***Fig. 13**: Simulation Results Showing a Magnified View of the Stator Flux Waveforms under Motor Mode at 1.2 pu Speed and 1 pu Load Torque.*

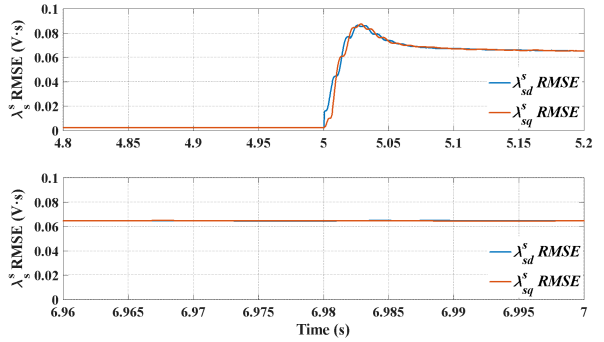

***Fig. 14**: Simulation Results Showing the Waveforms of RMS error of the Estimated Stator Flux: (Top) during a Step Change in Rotor Speed and (Bottom) under Steady-State Condition.*

the sampling and switching frequencies. Likewise, increase in the model order can also improve the results. However, there must be a trade-off between accuracy and computational cost.

The $\lambda^s_s RMSE$ of the stator flux in each axis is depicted in Fig. 14. The results shown in Fig. 14 consist of the $\lambda^s_s RMSE$ waveforms during transient and steady-state conditions. As depicted in Fig. 14, the steady-state RMS error is approximately 0.065 V·s corresponding to roughly 0.063 pu with respect to 1.0396 V·s flux base. This error can be reduced by increasing the sampling frequency or by increasing the order of the approximated model.

4.2.2 Step Change in Load Torque

The effect of a step change in load torque was observed by initially simulating the system under no-load conditions. A step change in load torque occurs at the time 7 s. as illustrated in Fig. 15. The results under steady-state conditions are shown in Fig. 16.

The step change in load torque from zero to 1 pu occurs at the time 7 s. As shown in this figure, the DFIM is still under control as can be seen in the waveforms of speed and electromagnetic torque. Considering the $\lambda^s_s RMSE$

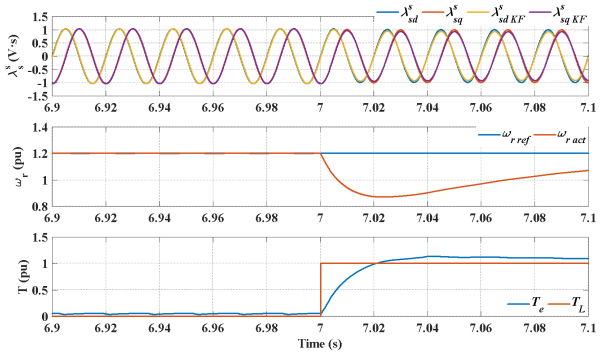

***Fig. 15**: Simulation Results Showing the Waveforms of the (Top) Stator Flux, (Middle) Rotor Speed, and (Bottom) Torque during a Step Change in Load.*

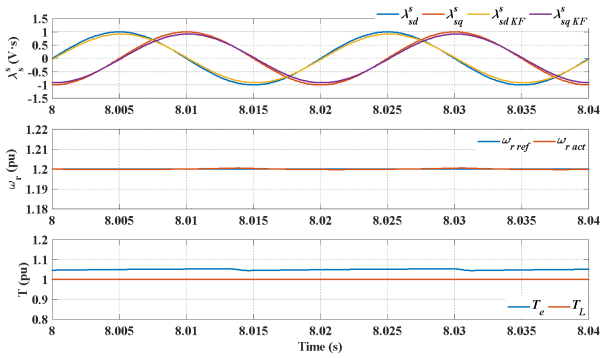

***Fig. 16**: Simulation Results Showing the Waveforms of the (Top) Stator Flux, (Middle) Rotor Speed, and (Bottom) Torque under Steady-State Motor Operation.*

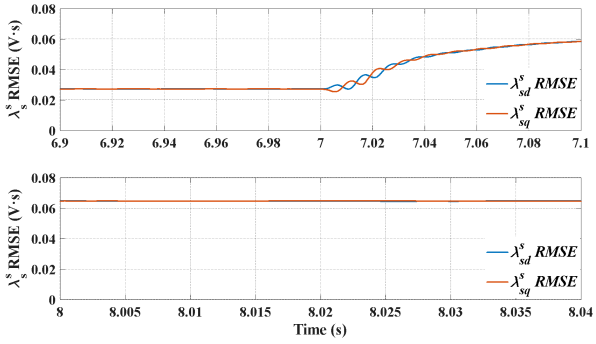

***Fig. 17**: Simulation Results Showing the Waveforms of RMS error of the Estimated Stator Flux: (Top) during a Step Change in Load and (Bottom) under Steady-State Condition.*

waveforms during transient at the top of Fig. 17, under no-load, the RMS error is approximately 0.027 V·s (0.026 pu) and its value changes to roughly 0.065 V·s (0.063 pu) at 1 pu load.

4.2.3 Operation in Generator Mode

The operation in generator mode is also considered. In this simulation, the DFIM initially operates in motor

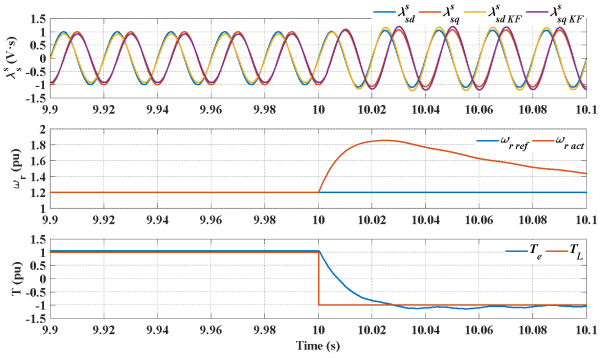

***Fig. 18**: Simulation Results Showing the Waveforms of the (Top) Stator Flux, (Middle) Rotor Speed, and (Bottom) Torque during a Step Change from Motor Mode to Generator Mode.*

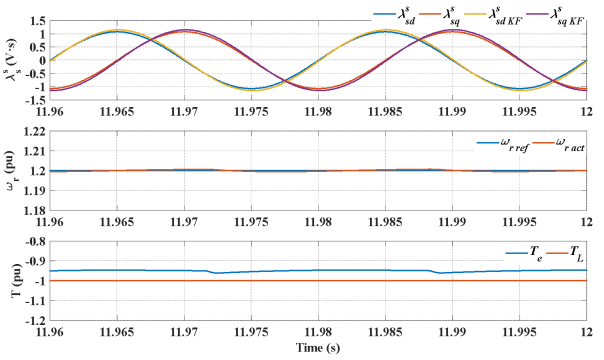

***Fig. 19**: Simulation Results Showing the Waveforms of the (Top) Stator Flux, (Middle) Rotor Speed, and (Bottom) Torque under Steady-State Generator Operation.*

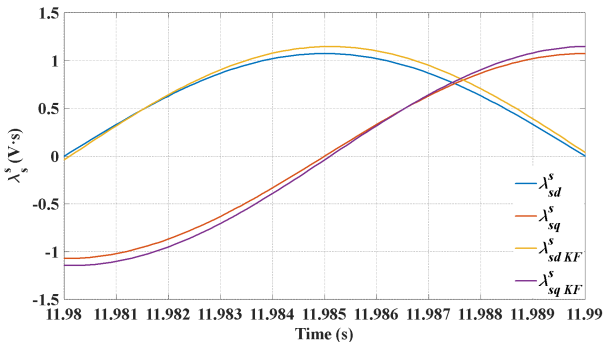

***Fig. 20**: Simulation Results Showing a Magnified View of the Stator Flux Waveforms under Generator Mode at 1.2 pu speed and 1 pu. Load Torque.*

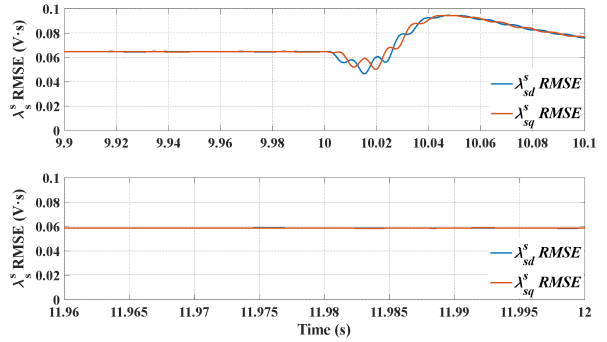

***Fig. 21**: Simulation Results Showing the Waveforms of RMS error of the Estimated Stator Flux: (Top) during a Step Change from Motor Mode to Generator Mode and (Bottom) under Steady-State Condition.*

mode with 1 pu load torque. At the time 10 s, the load torque is changed to -1 pu, forcing the DFIM to operate in generator mode. The simulation results during a step change in the operating mode are shown in Fig. 18. The estimated stator flux waveforms have the same response as the reference stator flux waveforms.

The steady-state results are shown in Fig.19. It can be observed that the amplitude of the estimated stator flux is slightly higher than that of the reference stator flux, as illustrated in the magnified view shown in Fig. 20. The $\lambda^s_S RMSE$ waveforms are depicted in Fig. 21. During generator operation, the RMS error is about 0.059 V·s (0.057 pu) which is slightly lower than that in motor mode.

4.2.4 Operation under Unbalanced Stator Voltage

Since the stator of the DFIM is directly connected to the grid, the appearance of unbalanced stator voltage causes pulsating torque and generates negative-sequence stator flux. Consequently, the estimated stator flux speed and position are distorted. Therefore, the DSOGI-PLL is adopted to extract the positive-sequence flux component for flux position and speed estimation. In the simulation, the voltage level of each phase is set to 248.26 V, 213.62 V and 225.17 V. This setup results in 232.9 V for the positive-sequence component and 14.4 V for the negative-sequence component. Therefore, according to IEC 60034-26 [38], the voltage unbalance factor is 4.45 %.

The simulation results shown in Figs. 22 are the waveforms during a step change in the speed command. During the step change in speed command, the flux speed distortion is mainly caused by the transient response. Once steady-state is reached, the estimated stator flux speed becomes smoother as shown in Fig. 23. It should be noted that the amplitude of the d- and q-components are not identical. This mismatch can result in distortion of the estimated stator flux speed and position. However, the distortion is mitigated by the DSOGI-PLL.

A similar phenomenon occurs in the case of a step change in the operating mode from motor mode to generator mode as illustrated in Figs. 24 and 25. However, the flux speed distortion is more prominent while operating in the generator mode.

The unbalanced voltage directly affects the output variables of the DFIM, such as an electromagnetic torque and rotor speed. Both speed and torque, as illustrated in Figs. 26 and 27, are oscillating at twice the stator fundamental frequency.

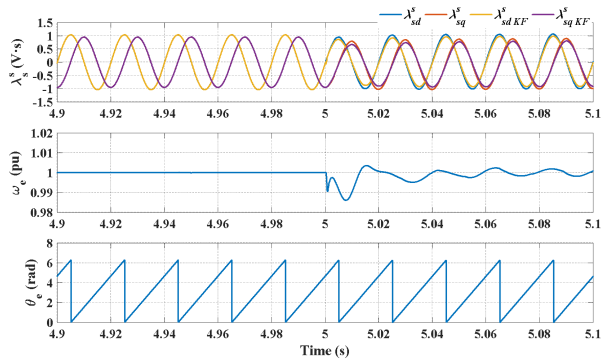

***Fig. 22**: Simulation Results Showing the Waveforms of the (Top) Stator Flux (Middle) Flux Speed and (Bottom) Flux Position during a Step Change in the Speed Command under Unbalanced Stator Voltage Condition.*

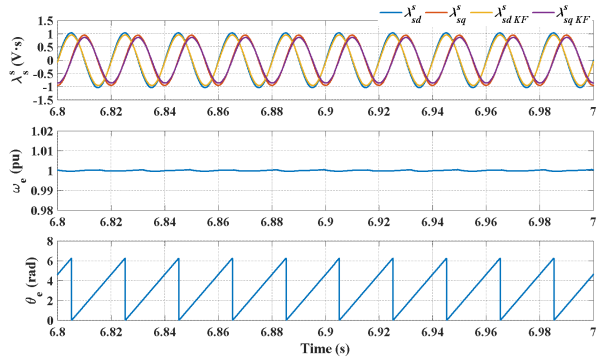

***Fig. 23**: Simulation Results Showing the Waveforms of the (Top) Stator Flux (Middle) Flux Speed and (Bottom) Flux Position in Motor Mode under Steady-State Unbalanced Stator Voltage Condition.*

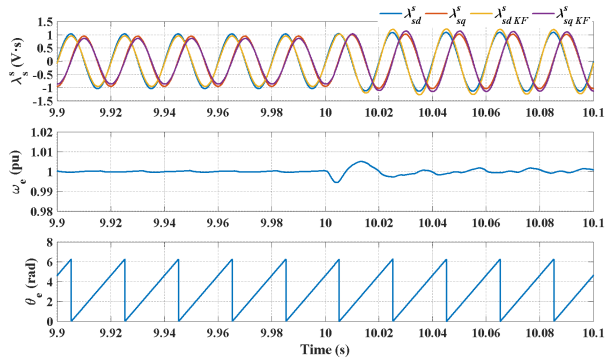

***Fig. 24**: Simulation Results Showing the Waveforms of the (Top) Stator Flux (Middle) Flux Speed and (Bottom) Flux Position during a Step Change in the Operating Mode under Unbalanced Stator Voltage Condition.*

It should also be observed what happens to the estimated flux position when the unbalanced voltage occurs. The simulation results depicted in Fig. 28 are the comparison of the stator flux position between the reference and the estimated stator flux based on the

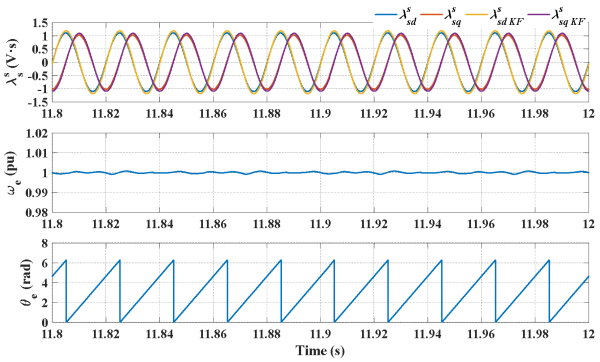

***Fig. 25**: Simulation Results Showing the Waveforms of the (Top) Stator Flux (Middle) Flux Speed and (Bottom) Flux Position in Generator Mode under Steady-State Unbalanced Stator Voltage Condition.*

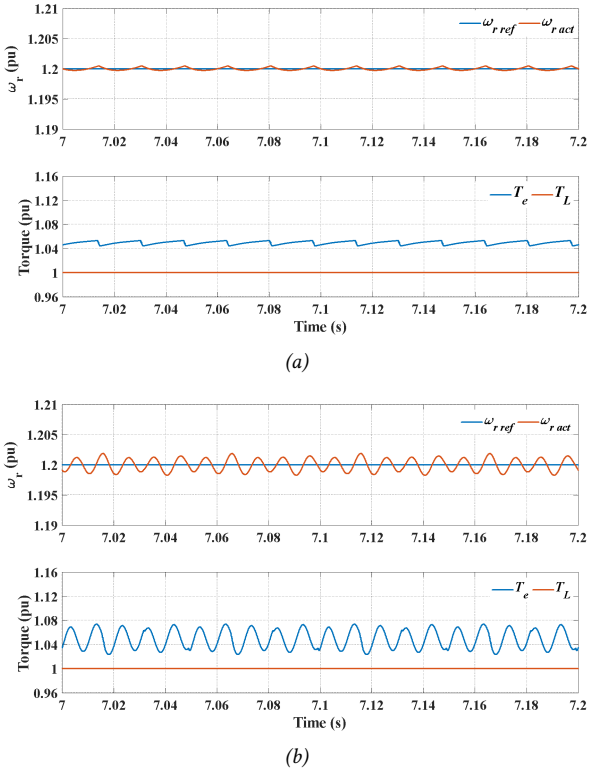

***Fig. 26**: Simulation Results Showing the Rotor Speed and Electromagnetic Torque Waveforms of the DFIM Operating in Motor Mode under (a) Balanced and (b) Unbalanced Voltage Conditions.*

DSOGI-PLL. In the comparison, the position of the reference flux is calculated using the "atan2" function. The comparison shown in Fig. 28a is the result under ideal conditions. The estimated position is as smooth as that of the reference. However, under unbalanced voltage conditions, the calculated position of the reference flux is highly distorted, while the estimated position using the DSOGI-PLL is smoother, as depicted in Fig. 28b.

As previously discussed in [36], during the opera-

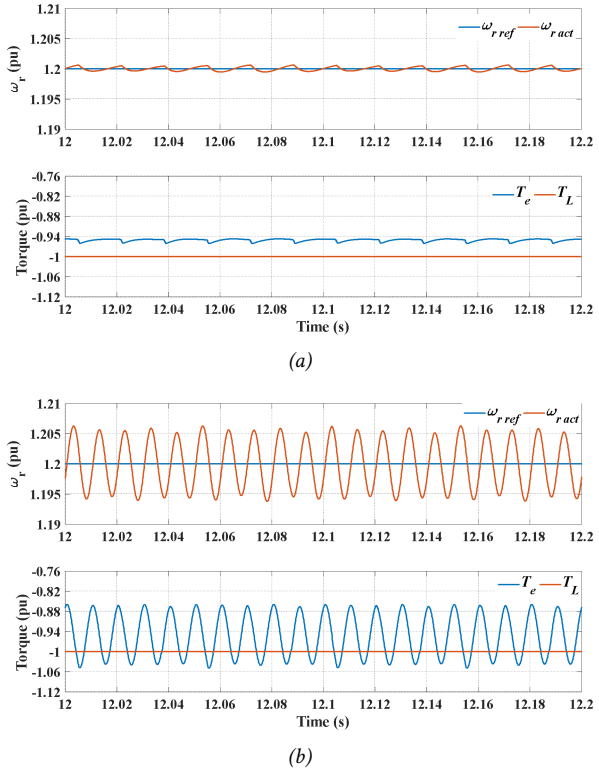

***Fig. 27**: Simulation Results Showing the Rotor Speed and Electromagnetic Torque Waveforms of the DFIM Operating in Generator Mode under (a) Balanced and (b) Unbalanced Voltage Conditions.*

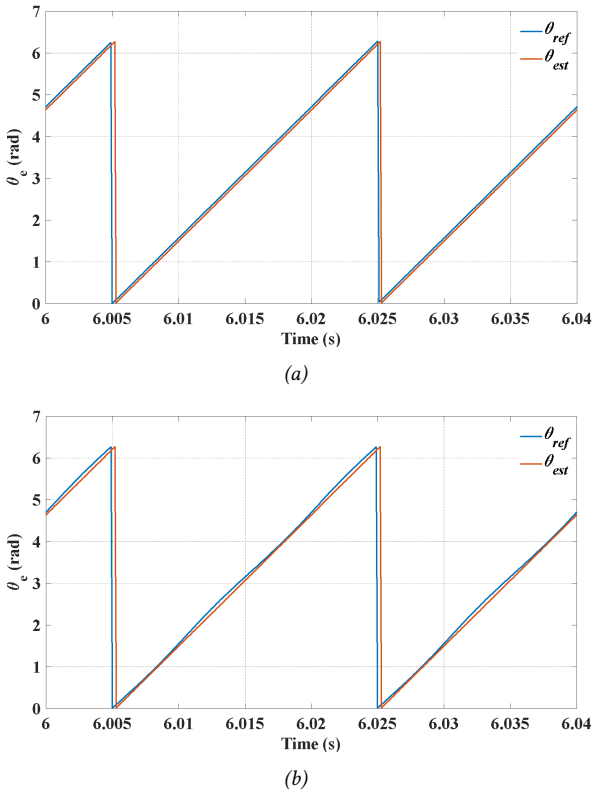

***Fig. 28**: Simulation Results Showing Comparison of Stator Flux Position from the Reference Model (Calculated Position) and DSOGI-PLL Estimate under (a) Balanced and (b) Unbalanced Voltage Conditions.*

tion without the DSOGI-PLL or other modified PLLs, the negative-sequence component appears in the stator current waveforms. Moreover, the rotor current is highly distorted, leading to high torque pulsation, which consequently damages the rotating part of the DFIM.

5. CONCLUSION

This paper presents the application of the Kalman filter for stator flux estimation for the DFIM. With the combination of the DFIM model and the measurement variables, the Kalman filter can estimate the stator flux vector that cannot be measured directly. The stator flux estimation scheme presented in this paper includes the DSOGI-PLL for extracting the positive-sequence components for smooth estimated stator flux speed and position.

The simulation system was created using PLECS software with the CMSIS-DSP library integrated in the C-Script. The CMSIS-DSP library can help perform the matrix manipulation required for Kalman filter calculation. The simulations were performed under different operating conditions, such as 1. step change in the speed command, 2. step change in load torque, 3. operation in generator mode and 4. operation under unbalanced stator voltage. For the first three conditions, the estimated stator flux waveforms have the same response as that of the reference flux waveforms. However, if there is an unbalanced stator voltage, the negative-sequence component occurs in the stator flux waveforms. Consequently, the estimated stator flux speed and position will also be distorted. Therefore, the DSOGI-PLL is applied to estimate the stator flux speed and position. The simulation results show that both stator flux speed and position waveform distortions are mitigated, maintaining the performance of the stator flux vector control for the DFIM.

Finally, it can be concluded that the proposed stator flux estimation scheme successfully estimates the stator flux vector for the DFIM under different operating conditions. The code applied in the simulation system can simply be transferred to the experimental system with little modification.

REFERENCES

[1] W. Leonhard. *Control of Electrical Drives*, 3rd ed. Berlin, Germany: Springer, 2001.

[2] P. Vas. *Vector Control of AC Machines*, UK: Oxford University Press, 1990.

[3] P. Vas. *Electrical Machines and Drives: A Space-Vector Theory Approach*, UK: Oxford University Press, 1993.

[4] P. Vas. *Sensorless Vector and Direct Torque Control*, UK: Oxford University Press, 1998.

[5] B.K. Bose. *Modern Power Electronics and AC Drives*, Prentice Hall 2001.

[6] Nguyen Phung Quang and Jörg-Andreas Dittrich, "*Vector Control of Three-Phase AC Machines*, Berlin, Heidelberg: Springer, 2015.

[7] D. J. Atkinson, P. P. Acarnley and J. W. Finch, "Observers for induction motor state and parameter estimation," *IEEE Transactions on Industry Applications*, vol. 27, no. 6, pp. 1119-1127, Nov.-Dec. 1991,

[8] Patrick L. Jansen and Robert D. Lorenz, "A Physical Insightful Approach to the Design and Accuracy Assessment of Flux Observers for Field Oriented Induction Machine Drives," *IEEE Transactions on Industry Applications*, vol. 30, No. 1, pp. 101-110, Jan.-Feb 1994.

[9] Cristian Lascu, Ion Boldea, and Frede Blaabjerg, "A Modified Direct Torque Control for Induction Motor Sensorless Drive," *IEEE Transactions on Industry Applications*, vol. 36, no. 1, pp. 122-130, Jan.-Feb 2000.

[10] J. Holtz, "Sensorless control of induction motor drives," in Proceedings of the IEEE, vol. 90, no. 8, pp. 1359-1394, Aug. 2002,

[11] R. Pena, J. C. Clare, and G. M. Asher, "Doubly-Fed Induction Generator Using Back-to-Back PWM Converters and Its Application to Variable Speed Wind-Energy Generation", *IEE Proceeding of Electric Power Applications*, vol. 143, no. 5, pp. 380-387, 1996.

[12] G. Tapia, G. Santamaria, M. Telleria, and A. Susperregui, "Methodology for Smooth Connection of Doubly Fed Induction Generators to the Grid," *IEEE Transactions on Energy Conversion*, vol. 24, no. 4, pp. 959-971, Dec 2009.

[13] X. Yuan, J. Chai, and Y. Li, "A Converter-Based Starting Method and Speed Control of Doubly-Fed Induction Machine with Centrifugal Loads," *IEEE Transaction on Industry Applications*, vol. 47, no. 3, pp. 1409–1418, May/Jun. 2011.

[14] Y. Pannatier, B. Kawkabani, C. Nicolet, A. Schwery and J. . -J. Simond, "Optimization of the Start-Up Time of a Variable Speed Pump-Turbine Unit in Pumping Mode," in *2012 XXth International Conference on Electrical Machines*, Marseille, France, 2012, pp. 2126-2132.

[15] T. Maendly, A. Hodder and B. Kawkabani, "Start-Up of a Varspeed Group in Pump Mode, Practical Implementations and Tests," in *2016 XXII International Conference on Electrical Machines (ICEM)*, Lausanne, Switzerland, 2016, pp. 1201-1207.

[16] [16] A. Joseph, R. Selvaraj, T. R. Chelliah, and S.V. Appa Sarma, "Starting and Braking of Large Variable Speed Hydrogenerating Unit Subjected to Converter and Sensor Faults," *IEEE Transactions on Industry Applications*, vol. 54, no. 4, pp. 3372–3382, Jul.-Aug. 2018.

[17] T. Zhao, D. Xiang and, and Y. Sheng, "An Approach to Start a Shaft Generator System Employing DFIM under Power Take Me Home Mode," in *2018 IEEE International Power Electronics and Application Conference and Exposition (PEAC)*, Shenzhen, China, 2018, pp. 1-5.

[18] G. C. Verghese and S. R. Sanders, "Observers for flux estimation in induction machines," *IEEE Transactions on Industrial Electronics*, vol. 35, no. 1, pp. 85-94, Feb. 1988.

[19] R. Cardenas, R. Pena, J. Proboste, G. Asher and J. Clare, "MRAS observer for sensorless control of standalone doubly fed induction generators," *IEEE Transactions on Energy Conversion*, vol. 20, no. 4, pp. 710-718, Dec. 2005.

[20] R. Cardenas, R. Pena, G. Asher, J. Clare and J. Cartes, "MRAS observer for doubly fed induction Machines," *IEEE Transactions on Energy Conversion*, vol. 19, no. 2, pp. 467-468, June 2004.

[21] R. Pena, R. Cardenas, J. Proboste, G. Asher and J. Clare, "Sensorless Control of Doubly-Fed Induction Generators Using a Rotor-Current-Based MRAS Observer," *IEEE Transactions on Industrial Electronics*, vol. 55, no. 1, pp. 330-339, Jan. 2008.

[22] M. S. Carmeli, F. Castelli-Dezza, M. Iacchetti and R. Perini, "Effects of Mismatched Parameters in MRAS Sensorless Doubly Fed Induction Machine Drives," *IEEE Transactions on Power Electronics*, vol. 25, no. 11, pp. 2842-2851, Nov. 2010.

[23] F. C. Dezza, G. Foglia, M. F. Iacchetti and R. Perini, "An MRAS Observer for Sensorless DFIM Drives with Direct Estimation of the Torque and Flux Rotor Current Components," *IEEE Transactions on Power Electronics*, vol. 27, no. 5, pp. 2576-2584, May 2012.

[24] M. F. Iacchetti, "Adaptive Tuning of the Stator Inductance in a Rotor-Current-Based MRAS Observer for Sensorless Doubly Fed Induction-Machine Drives," *IEEE Transactions on Industrial Electronics*, vol. 58, no. 10, pp. 4683-4692, Oct. 2011.

[25] R. Bhattarai, N. Gurung, S. Ghosh and S. Kamalasadan, "Parametrically Robust Dynamic Speed Estimation Based Control for Doubly Fed Induction Generator," *IEEE Transactions on Industry Applications*, vol. 54, no. 6, pp. 6529-6542, Nov.-Dec. 2018.

[26] P. Mondal, M. K. Malakar, P. Tripathy, S. Krishnaswamy and U. K. Saha, "Robust Observer Design for Sensorless Voltage and Frequency Control of a Doubly Fed Induction Generator in Standalone Mode," *IEEE Transactions on Energy Conversion*, vol. 37, no. 2, pp. 844-854, June 2022.

[27] Y. Mousavi, G. Bevan, I. B. Kucukdemiral and A. Fekih, "Observer-Based High-Order Sliding Mode Control of DFIG-Based Wind Energy Conversion Systems Subjected to Sensor Faults," *IEEE Trans-*

actions on Industry Applications, vol. 60, no. 1, pp. 1750-1759, Jan.-Feb. 2024.

[28] M. W. K. Mbukani and N. Gule, "PLL-Based Sliding Mode Observer Estimators for Sensorless Control of Rotor-Tied DFIG Systems," *IEEE Transactions on Industry Applications*, vol. 55, no. 6, pp. 5960-5970, Nov.-Dec. 2019.

[29] Dan Simon. *Optimal State Estimation Kalman, H_∞ and Nonlinear Approaches*, Wiley. 2006.

[30] Li-Cheng Zai, C. L. DeMarco and T. A. Lipo, "An extended Kalman filter approach to rotor time constant measurement in PWM induction motor drives," *IEEE Transactions on Industry Applications*, vol. 28, no. 1, pp. 96-104, Jan.-Feb. 1992,

[31] G. C. Verghese and S. R. Sanders, "Observers for flux estimation in induction machines," *IEEE Transactions on Industrial Electronics*, vol. 35, no. 1, pp. 85-94, Feb. 1988,

[32] L. Loron and G. Laliberte, "Application of the extended Kalman filter to parameters estimation of induction motors," in *1993 Fifth European Conference on Power Electronics and Applications*, Brighton, UK, 1993, pp. 85-90 vol.5.

[33] P. Rodríguez, R. Teodorescu, I. Candela, A. V. Timbus, M. Liserre and F. Blaabjerg, "New positive-sequence voltage detector for grid synchronization of power converters under faulty grid conditions," in *2006 37th IEEE Power Electronics Specialists Conference*, Jeju, Korea (South), 2006, pp. 1-7,

[34] Z. Ali, N. Christofides, L. Hadjidemetriou, E. Kyriakides, Y. Yang and F. Blaabjerg, "Three-phase Phase-Locked Loop Synchronization Algorithms for Grid-Connected Renewable Energy Systems: A Review," Renewable and Sustainable Energy Reviews, vol. 90, pp. 434-452, July 2018.

[35] W. Suwan-ngam, "Analysis of a Doubly-Fed Induction Motor for Soft Start Operation based on Stator Flux Vector Control," *ECTI Transactions on Electrical Engineering, Electronics, and Communications*, vol. 22, no. 3, Oct. 2024.

[36] K. Chaimanekorn and W. Suwan-ngam, "System Implementation for the Soft Start Operation of a Doubly-Fed Induction Motor," *ECTI Transactions on Electrical Engineering, Electronics, and Communications*, vol. 22, no. 3, Oct. 2024.

[37] D. Wilson, "Teaching Your PI Controller to Behave," TI Technical Article, July 2015.

[38] IEC, Rotating Electrical Machines — Part 26: Effects of Unbalanced Voltages on the Performance of Three-Phase Cage Induction Motors, IEC Standard 60034-26, 1st ed., Geneva, Switzerland, 2006, Corrigendum 1, Sept. 2014.

Jirawat Kodchaporn received the B.Eng. in Electrical Engineering from the King Mongkut's Institute of Technology Ladkrabang (KMITL), Bangkok, Thailand in 2023. He is currently pursuing an M.Eng degree at KMITL. His research interests include motor control, linear and nonlinear observers, and the application of embedded systems for digital signal processing. e-mail : HYPERLINK "mailto:66016019@kmitl.ac.th" 66016019@kmitl.ac.th

Warachart Suwan-ngam received the B.Eng. and M.Eng. in Electrical Engineering from the King Mongkut's Institute of Technology Ladkrabang (KMITL), Bangkok, Thailand in 1999 and 2002, respectively, and the Ph.D. in Electronic and Electrical Engineering from the University of Strathclyde, Glasgow, UK. in 2008. He is currently an Assistant Professor in the Department of Electrical Engineering, School of Engineering, KMITL. His research interests include electrical machines and AC drives, power electronics applications for renewable energy, condition monitoring and fault diagnosis for electrical machines and power converters, and DSP applications for AC drives and power electronics converters. e-mail: warachart.su@kmitl.ac.th